Nano Research 2016, 9(10): 3066–3074
DOI 10.1007/s12274-016-1189-4
Research Article
ISSN 1998-0124
CN 11-5974/O4

Sub-2.0-nm Ru and composition-tunable RuPt nanowire networks

Weiyue Zhao[1], Dabing Huang[1], Qiang Yuan[1] (✉), and Xun Wang[2] (✉)

[1] *College of Chemistry and Chemical Engineering, Guizhou University, Guiyang, Guiyang 550025, China*
[2] *Department of Chemistry, Tsinghua University, Beijing 100084, China*

Received: 23 March 2016
Revised: 16 June 2016
Accepted: 18 June 2016

KEYWORDS
Ru,
Pt,
alloy,
nanowire networks,
electrocatalysis

ABSTRACT

Recently, the synthesis of ultrathin nanostructures has attracted increasing interest because of their unique structure and properties. In this work, we report the synthesis of sub-2.0-nm Ru and composition-tunable RuPt nanowire networks using an environmentally friendly aqueous method. The structures were characterized using transmission electron microscopy (TEM), high-resolution TEM, X-ray diffraction (XRD), and energy-dispersive X-ray (EDX) spectroscopy. Moreover, the combined utilization of sodium n-dodecyl sulfate and potassium fluoride was determined to play a key role in the formation of these ultrathin nanostructures. The electrocatalytic properties of the sub-2.0-nm RuPt nanowire networks were investigated for methanol oxidation in an acidic medium. The nanostructures displayed composition-dependent properties, and compared with commercial $Ru_{50}Pt_{50}$/C, the as-synthesized $Ru_{56}Pt_{44}$ ultrathin nanowire network exhibited enhanced stability.

1 Introduction

Ru is a versatile element in the Pt group because of its robust roles in many laboratory and industrial applications such as hydrogenation, oxidation of alcohols, hydrogen generation, Fischer–Tropsch synthesis, biomass fuels, nitrogen fixation, and liquid fuel cells [1–7]. The size- and shape-controlled synthesis of metal nanocrystals has attracted extensive attention because of the intrinsic correlation between the structure and properties [8–13]. Compared with other Pt group metals such as Pt, Pd, and Rh, there has been no successful report on the synthesis of Ru nanocrystals with well-defined and controllable morphologies. Thus far, only the synthesis of a few sphere-like particles of Ru nanocrystals in organic media has been reported [14–18]. Recently, the synthesis of one-dimensional nanowires has attracted increasing interest because of their unique structure and properties [19–27]. Early studies on nanowires synthesized from solution systems [28–33] often focused on relatively large diameters (>5.0 nm). Until recently, reports on the synthesis of sub-2.0-nm nanowires in oleylamine systems were rare [34–36]. The synthesis of sub-2.0-nm

Address correspondence to Qiang Yuan, sci.qyuan@gzu.edu.cn; Xun Wang, wangxun@mail.tsinghua.edu.cn

nanowires remains a challenge because these structures are often only a few atoms thick and one unit cell in width.

In bottom-up, solution-based processes, surfactants and inorganic salts have often been exploited to tailor the size and shape of nanocrystals [37–40]. In this paper, we report a facile aqueous solution method for the synthesis of high-yield Ru networks consisting of ultrafine nanowires with sub-2.0-nm diameters in the presence of poly(vinylpyrrolidone) (PVP, M_W = 40,000), sodium n-dodecyl sulfate (SDS), and potassium fluoride (KF). To the best of our knowledge, this study represents the first time that sub-2.0-nm Ru nanowires have been prepared. In addition, this method can be easily extended to synthesize composition-tunable, sub-2.0-nm RuPt nanowire networks under the same synthetic conditions with the introduction of a Pt precursor. The electrocatalytic properties of the Ru and RuPt nanowire networks for methanol oxidation were also investigated, and the RuPt nanowire networks displayed composition-dependent electrocatalytic properties.

2 Experimental

In a typical synthesis, $RuCl_3$, PVP, SDS, and KF were dissolved in 8.0 mL of deionized water. The resulting homogeneous dark red solution was transferred to a 12-mL Teflon-lined stainless-steel autoclave. The sealed vessel was then heated at 180 ˚C for 24 h. Figure 1(a) and Fig. S1(a) in the Electronic Supplementary Material (ESM) present transmission electron microscopy (TEM) images of the as-synthesized Ru sample prepared at 180 ˚C for 24 h. These images clearly demonstrate that the products consist of networks of interconnecting ultrafine nanowires. The high-resolution TEM (HRTEM) images (Fig. 1(b) and Fig. S1(b) in the ESM) reveal that the nanowires with an average width of approximately 1.5 ± 0.2 nm are composed of single-crystalline and twin boundaries, and stacking faults are readily observed along the nanowires. Clear lattice fringes appear on the surface of the Ru nanowires. The interval between two lattice fringes was determined to be 0.21 nm, similar to the distance between (002) planes of hexagonal Ru (0.214 nm, JCPDS 06-0663) [8]. Figure 1(c) presents X-ray diffraction (XRD) patterns

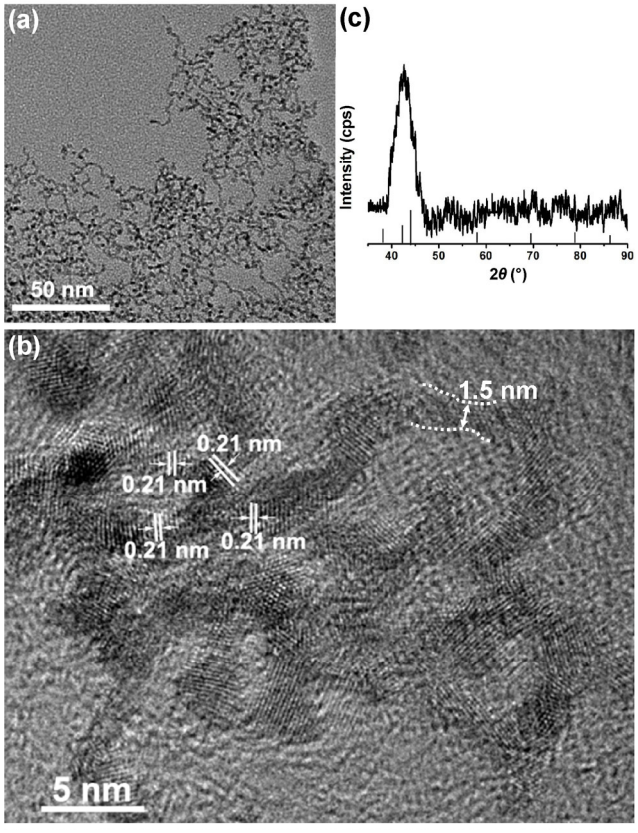

Figure 1 Representative TEM (a) and HRTEM (b) images of Ru nanowire networks synthesized at 180 ˚C for 24 h and XRD profile of as-synthesized products (c).

of the Ru nanowire networks. Only one peak is clearly observed at 42.3° in the XRD spectra, which was indexed to the (002) planes of hexagonal phase Ru (JCPDS 06-0663) and is consistent with the HRTEM analysis. Hexagonal-phase-pure Ru nanowires were also prepared and confirmed by Wong's group [31] using a polycarbonate membrane as a growth template and Ponrouch's group [41] using the porous structure of an anodic aluminum oxide membrane as the growth template.

3 Results and discussion

In the synthesis of metal nanostructures using PVP, PVP often plays dual roles as the reductant and surface-protecting agent because of the presence of the hydroxyl groups at the ends of PVP molecules [40]. Moreover, the coordinated use of both SDS and KF is vital to the formation of the Ru nanowire networks reported here. No products were obtained

from the reaction where SDS and KF were absent. Figure 2(a) and Fig. S2(a) in the ESM present typical TEM images obtained in the absence of KF. The products consisted of dominant ultrafine worm-like rods with diameters of less than 2.0 nm together with a small number of nanoparticles. In the absence of SDS, the products (Fig. 2(b) and Fig. S2(b) in the ESM) were similar to those obtained in the absence of KF. These results indicate that the SDS and KF tune the nuclei and growth rate of Ru nanocrystals, and high-yield Ru nanowire networks cannot be obtained in their absence. Many previous reports have indicated that halogen anions and surfactants control the morphology of metal nanocrystals by tuning the growth rate. For example, nanocubes can be obtained using Br^-, Pd, Pt, and Rh [42–44], and one-dimensional Pd [45], Pt [29], and Au [30, 34, 35] nanowires can be synthesized using I^- and alkylamine. To deepen the understanding of the effect of SDS and KF, a series of controlled experiments were performed by varying the SDS/KF molar ratio. Halving the SDS/KF molar ratio led to the formation of ultrafine worm-like rods together with a minority of branched nanowires and particles (Fig. 2(c)). In addition, doubling the SDS/KF molar ratio led to products consisting of shorter worm-like rods and more particles (Fig. 2(d)). These results indicate that the appropriate ratio of SDS/KF plays a key role in achieving high-yield Ru nanowire networks.

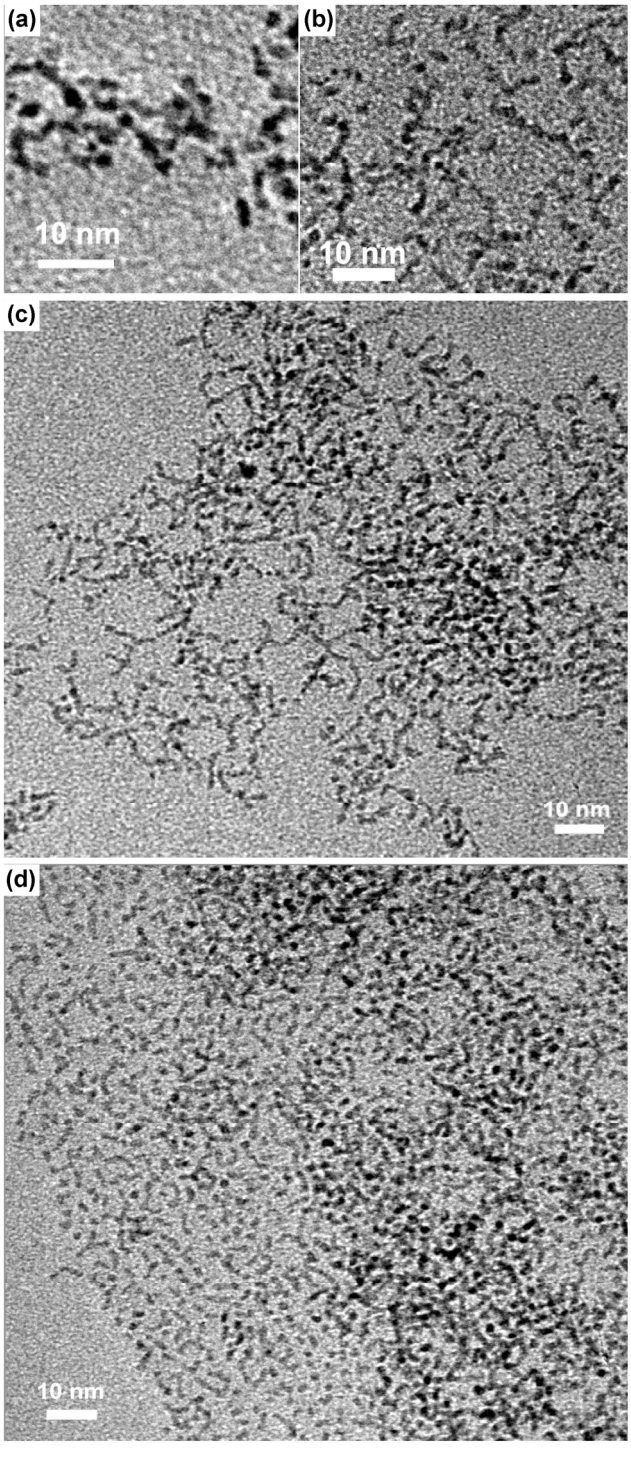

Figure 2 TEM images of Ru samples synthesized in the absence of KF (a) and SDS (b) and TEM images of Ru samples synthesized using SDS:KF mole ratios of (c) 1:1 and (d) 4:1.

A time evolutionary process is often used to clarify the formation mechanism of nanocrystals [30, 34, 45]. Figure 3(a) and Fig. S3(a) in the ESM present TEM images of the sample prepared with a reaction time of 6 h. The products were composed of ~2.0-nm-sized particles, and wires were not observed. Upon increasing the reaction time to 12 h, the products were composed of mixtures of particles and worm-like rods (Fig. 3(b) and Fig. S3(b) in the ESM). The number of particles was significantly reduced, the worm-like rods lengthened into worm-like wires, and branched wires appeared upon increasing the reaction time to 15 h (Fig. 3(c) and Fig. S3(c) in the ESM). The products were composed of longer wires with more and longer branches and nanowire networks upon further increasing the reaction time to 18 h (Fig. 3(d) and Fig. S3(d) in the ESM). These primary intermediates clearly demonstrate that the wires evolved from particles through the oriented-attachment mechanism (Fig. 3(e) and Fig. S4 in the ESM). This mechanism has been used to deduce the formation of nanowire network nanostructures

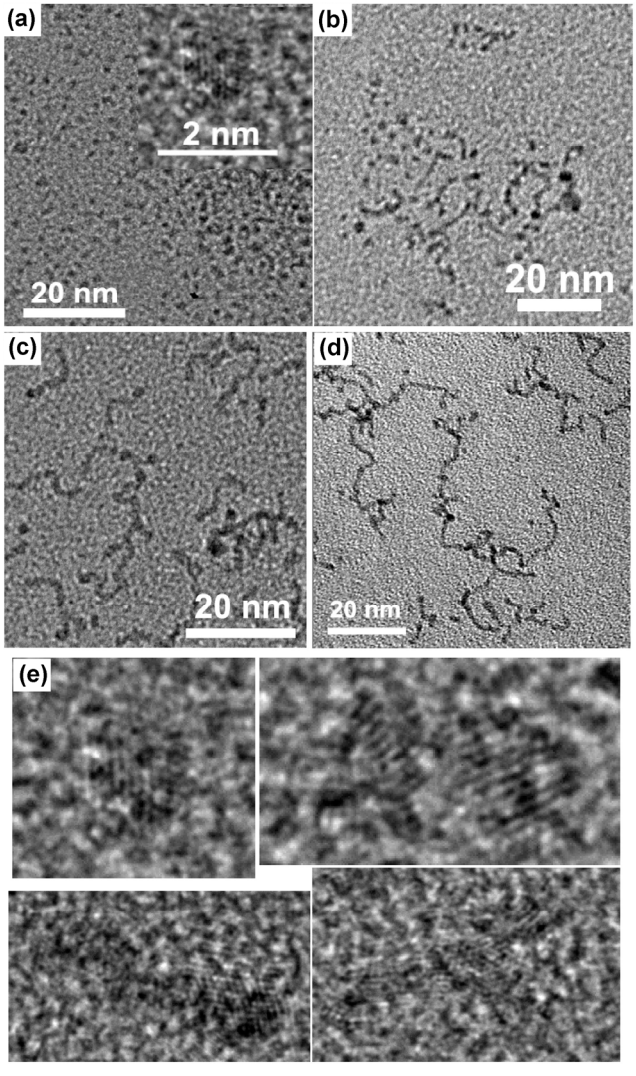

Figure 3 TEM images of Ru samples synthesized in reaction time of (a) 6 h, (b) 12 h, (c) 15 h, and (d) 18 h. (e) TEM images of initial intermediates.

synthesized from solution systems [23, 30, 46, 47], where nanowires are produced by oriented aggregation of faceted nanocrystals, and the total surface energy of the system decreases. Metal Ru has two crystal phases, namely the cubic phase and hexagonal phase. In our present synthetic route, hexagonal phase nanowires enclosed with {001} planes were obtained, as supported by the XRD analysis (Fig. 1(c)) and lattice fringe spacing (Fig. 1(b)). Based on these results, the formation of Ru nanowire networks is suggested to proceed via consecutive processes (Scheme 1). In the initial stage, the Ru^{3+} precursors were reduced and nucleated. Then, the nuclei grew to form sub-2.0-nm particles. The particles evolved to form rods, short

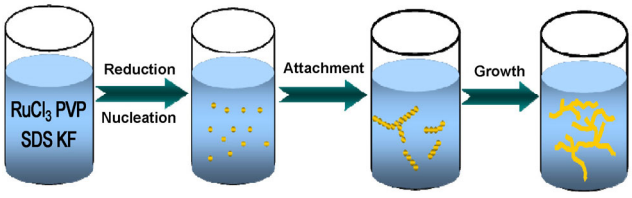

Scheme 1 Proposed formation mechanism of Ru nanowire networks.

wires, and nanowire networks, in sequence, preferentially along the growing <001> direction through oriented attachment. Furthermore, attachment possibly occurred along one of the {001} facets because all of the {001} facets are equivalent, which led to the formation of branched or circuited wires [30]. The oriented-attachment mechanism is also demonstrated by the lack of obvious width variation along the length direction during the growth process [23, 30] (Figs. 3(a)–3(d)) and the clear joining of two facets observed in the nanowires (Fig. 1(b) and Fig. S1(b)). Because the experiments were performed in a closed system, it remains challenging to unravel the growth mechanism of the nanowire networks.

Moreover, the present synthetic route can be easily extended to synthesize composition-tunable, sub-2.0-nm RuPt bimetal nanowire networks through the introduction of a Pt precursor (see the ESM for details). Figure S5(a) in the ESM presents TEM images of the as-synthesized RuPt bimetal alloy with a theoretical Ru/Pt molar ratio of 1:1. The product consists of nearly 100% selectivity of nanowires terminated with larger particles. The HRTEM images in Fig. 4(a) and Fig. S6 (in the ESM) indicate that the diameters of the nanowires and particles were 1.5 ± 0.2 nm and less than 5.2 nm, respectively. The surface lattice fringe interval of the particles and wires was determined to be 0.23 nm, which corresponds to the (111) facet of face-centered cubic (fcc) Pt. With increasing Ru content, the larger terminals gradually disappeared (Figs. 4(b)–4(d) and Figs. S5(b)–S5(d) in the ESM). When the theoretical Ru/Pt molar ratio increased to 2.4:1, the diameter of the terminals was nearly consistent with that of the wires (Fig. S5(d) in the ESM and Fig. 4(d)). Energy-dispersive X-ray spectroscopy (EDX) analysis (Fig. 5 and Table S1 in the ESM) indicated that these samples were composed of Ru and Pt. The composition of these as-synthesized RuPt nanowire networks could be tuned

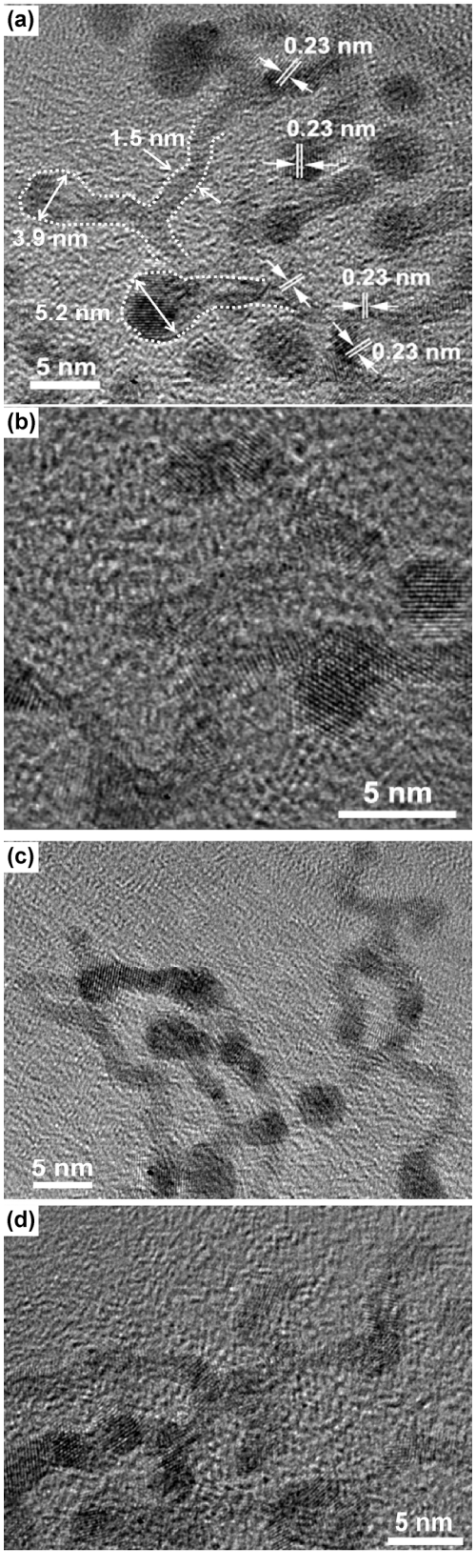

Figure 4 HRTEM images of RuPt nanowire networks prepared using Ru:Pt molar ratios of 1:1 (a), 1.2:1 (b), 1.8:1 (c), and 2.4:1 (d).

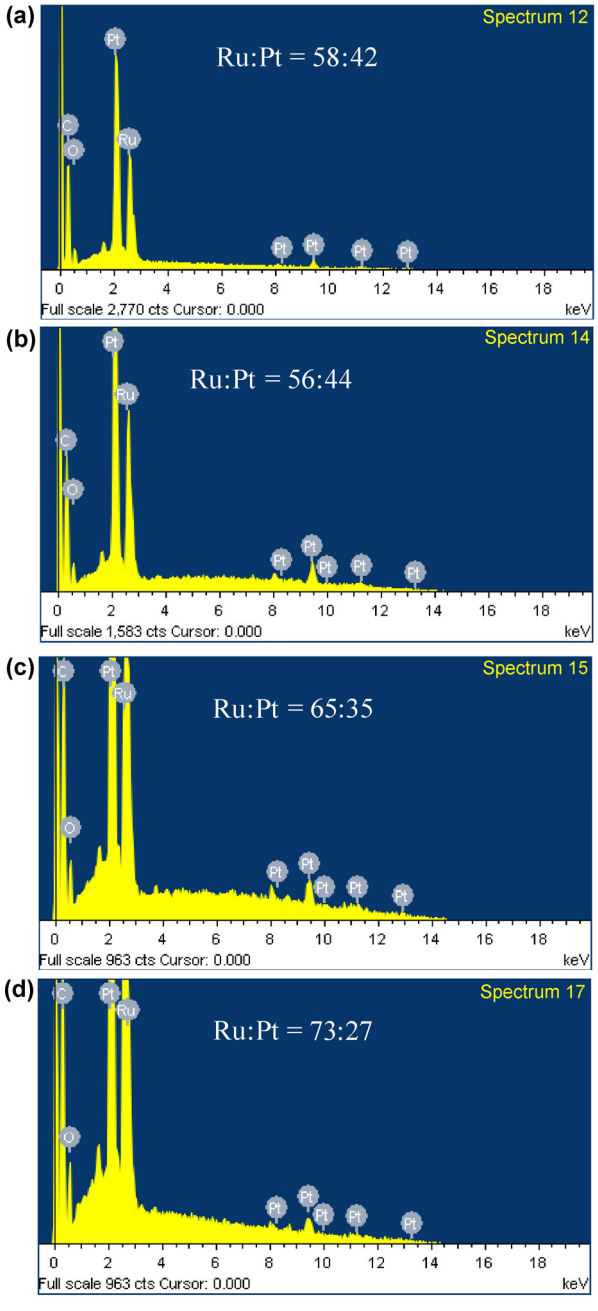

Figure 5 EDX spectra of RuPt nanowire networks prepared using Ru:Pt molar ratios of 1:1 (a), 1.2:1 (b), 1.8:1 (c), and 2.4:1 (d).

to $Ru_{58}Pt_{42}$, $Ru_{56}Pt_{44}$, $Ru_{65}Pt_{35}$, and $Ru_{73}Pt_{27}$. Figure S7 in the ESM presents an XRD pattern of the as-synthesized RuPt nanowire networks. The diffraction pattern can be readily indexed to the (111), (200), (220), and (311) planes of an fcc lattice and lies between those for pure Pt (JCPDS 65-2868) and Ru metals. Although the basal structure of Ru is hexagonal close-packed (hcp) (which is why pure Ru easily forms the hcp structure), Ru has another fcc structure [8, 48]. Therefore, when

Ru and Pt (Pt has an fcc structure) are coreduced, they have the potential to form an fcc structure. This observation indicates that Ru and Pt formed a solid-solution alloy. Electrochemical voltammetric methods can also provide overall structural information for catalysts. Figure S8(a) in the ESM presents the cyclic voltammograms of the Ru and RuPt nanowire alloys recorded in 0.5 M H_2SO_4. The hydrogen adsorption/desorption behaviors of the RuPt alloys are obviously different from that of single Ru. Furthermore, the element mapping analysis (Fig. S9 in the ESM) reveals that the Ru and Pt were well distributed in the nanowire networks. These results clearly indicate that Ru and Pt formed a solid-solution alloy.

RuPt alloys are often used as catalysts for methanol oxidation in liquid fuel cells [49]. Figure S8(b) in the ESM presents the steady-state cyclic voltammograms of the RuPt and Ru catalysts in a mixture of 1.0 M methanol and 0.5 M H_2SO_4 at 20 ˚C. The oxidation current was normalized to the electroactive surface area calculated using underpotential deposited Cu stripping techniques [50, 51], which is commonly used to assess the activity of RuPt catalysts. As shown in Fig. S8(b), the catalysts displayed composition-dependent catalytic performance. The peak current densities for the $Ru_{56}Pt_{44}$, $Ru_{58}Pt_{42}$, $Ru_{65}Pt_{35}$, and $Ru_{73}Pt_{27}$ nanowire networks were 0.26, 0.13, 0.15, and 0.14 mA·cm^{-2}, respectively. Among these structures, the $Ru_{56}Pt_{44}$ nanowire network catalyst exhibited the maximum catalytic activity, and the single Ru did not demonstrate catalytic activity for methanol oxidation. To evaluate the performance of the $Ru_{56}Pt_{44}$ nanowire network, the catalytic properties of commercial $Ru_{50}Pt_{50}$/C (80 wt.%, Johnson Matthey) were also tested under the same conditions. In the potential scan, the peak currents of the $Ru_{56}Pt_{44}$ nanowire network and commercial $Ru_{50}Pt_{50}$/C were 0.26 mA·cm^{-2} at 0.53 V and 0.3 mA·cm^{-2} at 0.48 V, respectively (Fig. 6(a)). Moreover, the mass activities of the $Ru_{56}Pt_{44}$ nanowire network and commercial $Ru_{50}Pt_{50}$/C were 167 and 198 mA·mg$_{Pt}^{-1}$, respectively (Fig. S8(c) in the ESM). The specific/mass activity on the $Ru_{56}Pt_{44}$ nanowire network was weaker than that on commercial $Ru_{50}Pt_{50}$/C (Figs. S8(b) and S8(c)). Long-term chronoamperometric experiments are often utilized to evaluate the electrocatalytic activity and stability of catalysts under continuous operating conditions [52]. Figure 6(b) presents the current vs. time curves recorded at 0.35 V for 1,800 s. Compared with the initial current density, 64% of the current density of the $Ru_{56}Pt_{44}$ nanowire network was maintained after 1,800 s, whereas only 39% of that of the commercial $Ru_{50}Pt_{50}$/C was maintained. Clearly, the final current density of the $Ru_{56}Pt_{44}$ nanowire network is higher than that of the commercial $Ru_{50}Pt_{50}$/C. Thus, the $Ru_{56}Pt_{44}$ nanowire network exhibited enhanced electrocatalytic stability. Moreover, after the oxidation test, the $Ru_{56}Pt_{44}$ retained its nanowire network morphology (Fig. S10 in the ESM).

4 Conclusions

In conclusion, for the first time, high-yield single Ru and composition-tunable RuPt alloy nanowire networks consisting of ultrafine nanowires with sub-2.0-nm widths were prepared using a one-pot, single aqueous

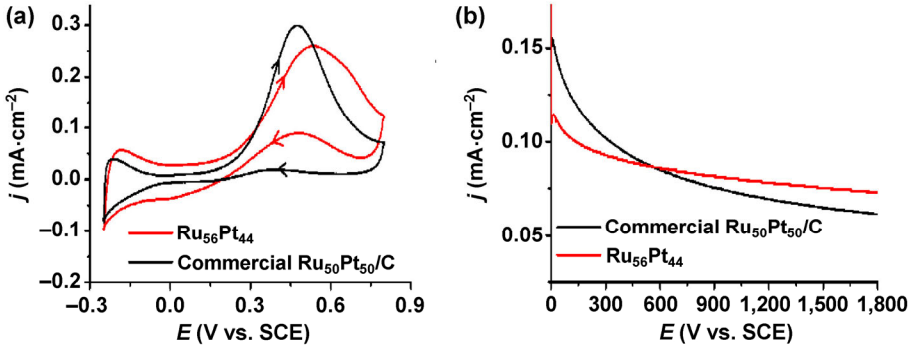

Figure 6 Electrocatalytic properties of as-synthesized $Ru_{56}Pt_{44}$ nanowire networks and commercial $Pt_{50}Ru_{50}$/C for methanol oxidation. (a) Steady-state cyclic voltammograms (50 mV·s^{-1}). (b) Current–time curves measured at 0.35 V in a mixture of 1.0 M methanol and 0.5 M H_2SO_4 at 20 ˚C.

phase method. Investigation of the formation mechanism clearly revealed that the nanowire networks were formed through particle attachment via consecutive processes including the formation of rods, short wires, and branched wires and that use of an appropriate SDS/KF ratio is a decisive factor. The electrocatalytic activity of these nanowire networks toward methanol oxidation was also investigated, with the results indicating that the RuPt nanowire networks displayed composition-dependent properties.

Acknowledgements

This work was supported by the National Natural Science Foundation of China (Nos. 21361005 and 21571038) and Graduate Innovation Foundation of Guizhou University (No. 2015031). The experimental work was mainly done in National University of Singapore and we also appreciate the useful discussion with Prof. Hua Chun Zeng of the National University of Singapore about this work.

Electronic Supplementary Material: Supplementary material (experimental details, additional TEM, HRTEM images, XRD patterns and electrocatalysis results) is available in the online version of this article at http://dx.doi.org/10.1007/s12274-016-1189-4.

References

[1] Zahmakıran, M.; Tonbul, Y.; Özkar, S. Ruthenium(0) nanoclusters stabilized by a nanozeolite framework: Isolable, reusable, and green catalyst for the hydrogenation of neat aromatics under mild conditions with the unprecedented catalytic activity and lifetime. *J. Am. Chem. Soc*. **2010**, *132*, 6541–6549.

[2] Anderson, R.; Griffin, K.; Johnston, P.; Alsters, P. L. Selective oxidation of alcohols to carbonyl compounds and carboxylic acids with platinum group metal catalysts. *Adv. Synth. Catal.* **2003**, *345*, 517–523.

[3] Fellay, C.; Dyson, P. J.; Laurenczy, G. A viable hydrogen-storage system based on selective formic acid decomposition with a ruthenium catalyst. *Angew. Chem., Int. Ed*. **2008**, *47*, 3966–3968.

[4] Xiao, C. X.; Cai, Z. P.; Wang, T.; Kou, Y.; Yan, N. Aqueous-phase Fischer–Tropsch synthesis with a ruthenium nanocluster catalyst. *Angew. Chem., Int. Ed*. **2008**, *47*, 746–749.

[5] Osada, M.; Sato, T.; Watanabe, M.; Adschiri, T.; Arai, K. Low-temperature catalytic gasification of lignin and cellulose with a ruthenium catalyst in supercritical water. *Energy Fuels* **2004**, *18*, 327–333.

[6] Nishibayashi, Y.; Iwai, S.; Hidai, M. Bimetallic system for nitrogen fixation: Ruthenium-assisted protonation of coordinated N_2 on tungsten with H_2. *Science* **1998**, *279*, 540–542.

[7] Kowal, A.; Li, M.; Shao, M.; Sasaki, K.; Vukmirovic, M. B.; Zhang, J.; Marinkovic, N. S.; Liu, P.; Frenkel, A. I.; Adzic, R. R. Ternary Pt/Rh/SnO_2 electrocatalysts for oxidizing ethanol to CO_2. *Nat. Mater*. **2009**, *8*, 325–330.

[8] Yin, A.-X.; Liu, W.-C.; Ke, J.; Zhu, W.; Gu, J.; Zhang, Y.-W.; Yan, C.-H. Ru nanocrystals with shape-dependent surface-enhanced Raman spectra and catalytic properties: Controlled synthesis and DFT calculations. *J. Am. Chem. Soc*. **2012**, *134*, 20479−20489.

[9] Nosheen, F.; Zhang, Z. C.; Xiang, G. L.; Xu, B.; Yang, Y.; Saleem, F.; Xu, X. B.; Zhang, J. C.; Wang, X. Three-dimensional hierarchical Pt–Cu superstructures. *Nano Res*. **2015**, *8*, 832–838.

[10] Zheng, F. L.; Wong, W.-T.; Yung, K.-F. Facile design of Au@Pt core–shell nanostructures: Formation of Pt submonolayers with tunable coverage and their applications in electrocatalysis. *Nano Res*. **2014**, *7*, 410–417.

[11] Alayoglu, S.; Nilekar, A. U.; Mavrikakis, M.; Eichhorn, B. Ru–Pt core–shell nanoparticles for preferential oxidation of carbon monoxide in hydrogen. *Nat. Mater*. **2008**, *7*, 333–338.

[12] Zhang, Q.; Guo, X.; Liang, Z. X.; Zeng, J. H.; Yang, J.; Liao, S. J. Hybrid PdAg alloy–Au nanorods: Controlled growth, optical properties and electrochemical catalysis. *Nano Res*. **2013**, *6*, 571–580.

[13] Xiang, J.; Li, P.; Chong, H. B.; Feng, L.; Fu, F. Y.; Wang, Z.; Zhang, S. L.; Zhu, M. Z. Bimetallic Pd–Ni core–shell nanoparticles as effective catalysts for the Suzuki reaction. *Nano Res*. **2014**, *7*, 1337–1343.

[14] Wang, Y.; Ren, J. W.; Deng, K.; Gui, L. L.; Tang, Y. Q. Preparation of tractable platinum, rhodium, and ruthenium nanoclusters with small particle size in organic media. *Chem. Mater*. **2000**, *12*, 1622–1627.

[15] Pan, C.; Pelzer, K.; Philippot, K.; Chaudret, B.; Dassenoy, F.; Lecante, P.; Casanove, M. J. Ligand-stabilized ruthenium nanoparticles: Synthesis, organization, and dynamics. *J. Am. Chem. Soc*. **2001**, *123*, 7584–7593.

[16] Yan, X. P.; Liu, H. F.; Liew, K. Y. Size control of polymer-stabilized ruthenium nanoparticles by polyol reduction. *J. Mater. Chem*. **2001**, *11*, 3387–3391.

[17] Viau, G.; Brayner, R.; Poul, L.; Chakroune, N.; Lacaze, E.;

Fiévet-Vincent, F.; Fiévet, F. Ruthenium nanoparticles: Size, shape, and self-assemblies. *Chem. Mater.* **2003**, *15*, 486–494.

[18] Tsukatani, T.; Fujihara, H. New method for facile synthesis of amphiphilic thiol-stabilized ruthenium nanoparticles and their redox-active ruthenium nanocomposite. *Langmuir* **2005**, *21*, 12093–12095.

[19] Zhai, H. T.; Wang, R. R.; Wang, W. Q.; Wang, X.; Cheng, Y.; Shi, L. J.; Liu, Y. Q.; Sun, J. Novel fabrication of copper nanowire/cuprous oxidebased semiconductor-liquid junction solar cells. *Nano Res*. **2015**, 8, 3205–3215.

[20] Yuan, J. K.; Liu, X. G.; Akbulut, O.; Hu, J. Q.; Suib, S. L.; Kong, J.; Stellacci, F. Superwetting nanowire membranes for selective absorption. *Nat. Nanotechnol*. **2008**, *3*, 332–336.

[21] Nerowski, A.; Opitz, J.; Baraban, L.; Cuniberti, G. Bottom-up synthesis of ultrathin straight platinum nanowires: Electric field impact. *Nano Res*. **2013**, *6*, 303–311.

[22] Cheng, H.; Lu, Z. G.; Deng, J. Q.; Chung, C. Y.; Zhang, K. L.; Li, Y. Y. A facile method to improve the high rate capability of Co_3O_4 nanowire array electrodes. *Nano Res*. **2010**, *3*, 895–901.

[23] Yuan, Q.; Zhou, Z. Y.; Zhuang, J.; Wang, X. Seed displacement, epitaxial synthesis of Rh/Pt bimetallic ultrathin nanowires for highly selective oxidizing ethanol to CO_2. *Chem. Mater.* **2010**, *22*, 2395–2402.

[24] Yang, S. C.; Hong, F.; Wang, L. Q.; Guo, S. W.; Song, X. P.; Ding, B. J.; Yang, Z. M. Ultrathin Pt-based alloy nanowire networks: Synthesized by CTAB assistant two-phase water−chloroform micelles. *J. Phys. Chem. C* **2010**, *114*, 203–207.

[25] Hu, S.; Liu, H. L.; Wang, P. P.; Wang, X. Inorganic nano-structures with sizes down to 1 nm: A macromolecule analogue. *J. Am. Chem. Soc*. **2013**, *135*, 11115–11124.

[26] Huang, X. Q.; Zhao, Z. P.; Chen, Y.; Chiu, C.-Y.; Ruan, L. Y.; Liu, Y.; Li, M. F.; Duan, X. F.; Huang, Y. High density catalytic hot spots in ultrafine wavy nanowires. *Nano Lett*. **2014**, *14*, 3887–3894.

[27] Scofield, M. E.; Koenigsmann, C.; Wang, L.; Liu, H. Q.; Wong, S. S. Tailoring the composition of ultrathin, ternary alloy PtRuFe nanowires for the methanol oxidation reaction and formic acid oxidation reaction. *Energy Environ. Sci*. **2015**, *8*, 350–363.

[28] Song, Y. J.; Garcia, R. M.; Dorin, R. M.; Wang, H. R.; Qiu, Y.; Coker, E. N.; Steen, W. A.; Miller, J. E.; Shelnutt, J. A. Synthesis of platinum nanowire networks using a soft template. *Nano Lett*. **2007**, *7*, 3650–3655.

[29] Teng, X. W.; Han, W.-Q.; Ku, W.; Hücker, M. Synthesis of ultrathin palladium and platinum nanowires and a study of their magnetic properties. *Angew. Chem., Int. Ed*. **2008**, *47*, 2055–2058.

[30] Halder, A.; Ravishankar, N. Ultrafine single-crystalline gold nanowire arrays by oriented attachment. *Adv. Mater*. **2007**, *19*, 1854–1858.

[31] Koenigsmann, C.; Semple, D. B.; Sutter, E.; Tobierre, S. E.; Wong, S. S. Ambient synthesis of high-quality ruthenium nanowires and the morphology-dependent electrocatalytic performance of platinum-decorated ruthenium nanowires and nanoparticles in the methanol oxidation reaction. *ACS Appl. Mater. Interfaces* **2013**, *5*, 5518–5530.

[32] Teng, X. W.; Feygenson, M.; Wang, Q.; He, J. Q.; Du, W. X.; Frenkel, A. I.; Han, W. Q.; Aronson, M. Electronic and magnetic properties of ultrathin Au/Pt nanowires. *Nano Lett.* **2009**, *9*, 3177–3184.

[33] Hong, X.; Tan, C.; Chen, J.; Xu, Z.; Zhang, H. Synthesis, properties and applications of one- and two-dimensional gold nanostructures. *Nano Res*. **2015**, *8*, 40–55.

[34] Huo, Z. Y.; Tsung, C. K.; Huang, W. Y.; Zhang, X. F.; Yang, P. D. Sub-two nanometer single crystal Au nanowires. *Nano Lett*. **2008**, *8*, 2041–2044.

[35] Lu, X. M.; Yavuz, M. S.; Tuan, H.; Korgel, B. A.; Xia, Y. N. Ultrathin gold nanowires can be obtained by reducing polymeric strands of oleylamine-AuCl complexes formed via aurophilic interaction. *J. Am. Chem. Soc*. **2008**, *130*, 8900–8901.

[36] Huo, Z. Y.; Tsung, C. K.; Huang, W. Y.; Fardy, M.; Yan, R. X.; Zhang, X. F.; Li, Y. D.; Yang, P. D. Self-organized ultrathin oxide nanocrystals. *Nano Lett*. **2009**, *9*, 1260–1264.

[37] Peng, X. G.; Manna, L.; Yang, W. D.; Wickham, J.; Scher, E.; Kadavanich, A.; Alivisatos, A. P. Shape control of CdSe nanocrystals. *Nature* **2000**, *404*, 59–61.

[38] Wang, D. S.; Peng, Q.; Li, Y. D. Nanocrystalline intermetallics and alloys. *Nano Res.* **2010**, *3*, 574–580.

[39] Liu, L. P.; Zhuang, Z. B.; Xie, T.; Wang, Y. G.; Li, J.; Peng, Q.; Li, Y. D. Shape control of CdSe nanocrystals with zinc blende structure. *J. Am. Chem. Soc*. **2009**, *131*, 16423–16429.

[40] Xiong, Y. J.; Washio, I.; Chen, J. Y.; Cai, H. G.; Li, Z. Y.; Xia, Y. N. Poly(vinyl pyrrolidone): A dual functional reductant and stabilizer for the facile synthesis of noble metal nanoplates in aqueous solutions. *Langmuir* **2006**, *22*, 8563–8570.

[41] Ponrouch, A.; Garbarino, S.; Pronovost, S.; Taberna, P.-L.; Simon, P.; Guay, D. Electrodeposition of arrays of Ru, Pt, and PtRu alloy 1D metallic nanostructures. *J. Electrochem. Soc*. **2010**, *157*, K59−K65.

[42] Zhang, Y. W.; Grass, M. E.; Kuhn, J. N.; Tao, F.; Habas, S. E.; Huang, W. Y.; Yang, P. D.; Somorjai, G. A. Highly selective synthesis of catalytically active monodisperse rhodium nanocubes. *J. Am. Chem. Soc*. **2008**, *130*, 5868–

5869.

[43] Tsung, C. K.; Kuhn, J. N.; Huang, W. Y.; Aliaga, C.; Hung, L. I.; Somorjai, G. A.; Yang, P. D. Sub-10 nm platinum nanocrystals with size and shape control: Catalytic study for ethylene and pyrrole hydrogenation. *J. Am. Chem. Soc.* **2009**, *131*, 5816–5822.

[44] Yuan, Q.; Zhuang, J.; Wang, X. Single-phase aqueous approach toward Pd sub-10 nm nanocubes and Pd–Pt heterostructured ultrathin nanowires. *Chem. Commun*. **2009**, 6613–6615.

[45] Huang, X. Q.; Zheng, N. F. One-pot, high-yield synthesis of 5-fold twinned Pd nanowires and nanorods. *J. Am. Chem. Soc*. **2009**, *131*, 4602–4603.

[46] Tang, Z. Y.; Kotov, N. A.; Giersig, M. Spontaneous organization of single CdTe nanoparticles into luminescent nanowire. *Science* **2002**, *297*, 237–240.

[47] Whang, D.; Jin, S.; Wu, Y.; Lieber, C. M. Large-scale hierarchical organization of nanowire arrays for integrated nanosystems. *Nano Lett*. **2003**, *3*, 1255–1259.

[48] Häglund, J.; Fernández Guillermet, A.; Grimvall, G.; Körling, M. Theory of bonding in transition-metal carbides and nitrides. *Phys. Rev. B* **1993**, *48*, 11685–11691.

[49] Chen, A. C.; Holt-Hindle, P. Platinum-based nanostructured materials: Synthesis, properties, and applications. *Chem. Rev*. **2010**, *110*, 3767–3804.

[50] Green, C. L.; Kucernak, A. Determination of the platinum and ruthenium surface areas in platinum−ruthenium alloy electrocatalysts by underpotential deposition of copper. I. Unsupported catalysts. *Phys. Chem. B* **2002**, *106*, 1036–1047.

[51] Jiang, J. H.; Kucernak, A. Mesoporous microspheres composed of PtRu alloy. *Chem. Mater*. **2004**, *16*, 1362–1367.

[52] Herrero, E.; Franaszczuk, K.; Wieckowski, A. Electrochemistry of methanol at low index crystal planes of platinum: An integrated voltammetric and chronoamperometric study. *Phys. Chem*. **1994**, *98*, 5074–5083.